Original paper

Low-overvoltage approach for reduction of the analytical volume in electron probe microanalysis: A case study of sulfide assemblages in enstatite-rich meteorites

Noemi MÉSZÁROSOVÁ^{1,2*}, Roman SKÁLA^{1,2}

- ¹ Institute of Geochemistry, Mineralogy and Mineral Resources, Faculty of Science, Charles University, Albertov 6, 128 43 Praha 2, Czech Republic
- ² Institute of Geology of the Czech Academy of Sciences, Rozvojová 269, 165 00 Praha 6, Czech Republic; meszarosova@gli.cas.cz
- *Corresponding author



Among enstatite-rich meteorites are included enstatite chondrites and enstatite achondrites (aubrites). The reducing conditions of origin are reflected in their mineralogy. Due to the lack of oxygen-bearing mineral assemblages allowing the application of traditional geothermometers, sulfides are used as a tool to constrain the conditions of their origin. In general, sulfide-based geothermometers rely on the contents of major or minor elements traditionally determined by electron probe microanalysis. This method requires the analyzed material to be a homogenous single phase in the analytical volume. However, sulfides of enstatite-rich meteorites frequently contain tiny lamellar inclusions of different phases, and therefore, the inclusions might affect the overall composition of sulfides. Consequently, the results of such analyses might influence the estimates of the conditions under which the given meteorite formed. This study discusses the effect of using the low-overvoltage approach to analyze iron and nickel (10 kV) in the primary sulfides of enstatiterich meteorites and how results compare to those obtained with the traditional analytical protocol (20 kV). The sulfides analyzed included Cr-Ti-bearing troilite, daubréelite (FeCr,S₄), and (Mg,Fe,Mn)S-monosulfide. Unfortunately, troilite often contains lamellar inclusion of daubréelite. Moreover, troilite inclusions are occasionally also included in (Mg,Fe,Mn) S-monosulfide. Therefore, obtaining an unbiased analysis of these minerals is intricate. Due to this, the main objective of using a lower accelerating voltage is to reduce the analytical volume to the minimum to increase the probability of avoiding tiny inclusions. Even if the analytical volume is inclusion-free, another complication might occur as the analysis of troilite may be affected by the neighboring daubréelite due to boundary fluorescence. Consequently, both phenomena bias the Cr content measured in troilite similarly, and due to the complexity of troilite-daubréelite assemblage, it is nearly impossible to quantify the amount of Cr content unbiased. Subsequently, to obtain the best possible dataset, precise sample screening and careful analytical point location setting are required in general. Using lower accelerating voltage brings many advantages as it allows better observation of the inclusions, and due to reducing the analytical volume, it reduces the chance of the presence of inclusions and suppresses the bias in Cr from boundary fluorescence. However, it also has disadvantages as the analysis is not trivial and does not favor trace elements analysis in general. Results demonstrate the importance of point-by-point inspection of the acquired data and subsequent elimination of biased analyses from the final datasets.

Keywords: Electron probe microanalysis, low-overvoltage approach, enstatite-rich meteorites, Cr-Ti bearing troilite, daubréelite, (Mg,Fe,Mn)S-monosulfide

Received: 18 February 2025; accepted: 5 May 2025; handling editor: J. Sejkora

The online version of this article (doi: 10.3190/jgeosci.402) contains electronic supplementary material.

1. Introduction

In general, meteorites are divided into two principal groups: undifferentiated and differentiated; the former – also called chondrites – did not undergo marked melting, and the latter underwent melting differentiation due to magmatic or metamorphic processes.

Enstatite-rich meteorites include undifferentiated enstatite chondrites and differentiated enstatite achondrites (aubrites). Enstatite chondrites are subdivided into two groups according to their bulk iron concentration: EH (high iron) and EL (low iron). Petrologic types within both

groups range from type 3 to type 6, meaning that enstatite chondrites may be pristine (type 3) to highly thermally metamorphosed (type 6). Among the enstatite chondrites, some meteorites are also classified as intermediate between the EH and EL groups, and some are impact-melt rocks or impact-melt breccias (Mason 1966; Keil 1986, 2007; Lin and Kimura 1998; Weisberg and Kimura 2012; Weyrauch et al. 2018; Lin 2022 and references therein).

Aubrites belong to a relatively rare group of differentiated meteorites, accounting for ~ 0.1 % of the known meteorite record, based on the data in the Meteoritical Bulletin Database (https://www.lpi.usra.edu/meteor/).

They are fragmental breccias, regolith breccias, and unbrecciated rocks formed by igneous processes. The magmatism producing aubrites is the most reducing known in the Solar System so far. In the past, the discussion about their common origin with enstatite chondrites was ongoing; it has recently settled on no common origin (Keil 1969; Watters and Prinz 1979; Brett and Keil 1986; Keil 2010). Aubrites are suggested to form on the parent body of an enstatite chondrite-like precursor and, together with the enstatite chondrite impact-melt breccias and impactmelt rocks, are considered petrologically analogous to Mercury (Udry et al. 2019; Wilbur et al. 2022).

Enstatite-rich meteorites are all believed to have formed in the innermost region of the protoplanetary disk. As reflected in their mineralogy, they formed in an environment with very low oxygen fugacity (Baedecker and Wasson 1975; Kallemeyn and Wason 1986). Due to the highly reducing conditions of origin, they contain nearly pure end-member enstatite (MgSiO₂), Si-bearing Fe-Ni-metal, phosphides like schreibersite (tetragonal (Fe,Ni)₂P), and sulfides of otherwise lithophile elements such as magnesium, calcium, chromium, titanium, etc. Among others, these sulfides include daubréelite (FeCr₂S₄), Cr-Ti-bearing troilite (FeS), and (Mg,Fe,Mn)S-monosulfide solid solution defined by the end members niningerite (MgS), alabandite (MnS), and keilite ($Fe_{>0.5}Mg_{<0.5}S$). The presence of niningerite is restricted to EH, while the presence of alabandite is exclusive to the EL. Keilite occurs in impact-related enstatite chondrites (Keil and Snetsinger 1967; Keil 1986, 2007; Lin 2022). From aubrites, only alabandite, often referred to as ferroan alabandite due to elevated Fe concentration, was reported (Watters and Prinz 1979; Kimura et al. 1993; Keil 2010; Wilbur et al. 2022).

Sulfide chemical composition and mutual relationships of sulfides may help to constrain the conditions of origin of the enstatite-rich meteorites (Lin and El Goresy 2002; Keil 2007, 2010; Weisberg and Kimura 2012; Horstmann et al. 2014; Kimura et al. 2017, 2021; Wilbur et al. 2022). However, these parameters are often obscured by the common presence of exsolution lamellas. Within troilite grains, exsolution lamellas of daubréelite of variable width commonly occur, which may vary from very fine submicron-sized lamellas to very wide 100 µm across lamellas, or daubréelite may appear as discrete grains adjacent to troilite. Moreover, the width of the exsolution lamellas may vary within one troilite-daubréelite assemblage. Rarely the exsolution lamellas of (Mg,Fe,Mn)Smonosulfide parallel to daubréelite lamellas are observed in troilite grains (Keil and Andersen 1965; Keil 1986; Lin and El Goresy 2002; Patzer et al. 2004; van Niekerk et al. 2014; Kimura et al. 2017; Weyrauch et al. 2018; Lin 2022). In some cases, the exsolution lamellas of troilite within the (Mg,Fe,Mn)S-monosulfide grains are observed (Keil and Fredriksson 1963; Keil and Andersen 1965; Lin

and El Goresy 2002; van Niekerk et al. 2014; Udry et al. 2019; Wilbur et al. 2022).

In aubrites, sulfides represent only a minor to trace component (Keil 2010; Udry et al, 2019; Wilbur et al. 2022). Due to the scarcity of sulfide grains, should petrologic implications be drawn, it is essential to characterize as many of them as possible. However, sulfide grains are usually tiny, which sometimes even prevents successful electron probe microanalysis (EPMA).

Electron probe microanalysis (EPMA) has had a significant impact on geological sciences since its development in the early 1950s by Raimond Castaing (Castaing 1951; McGee and Keil 2001). It became necessary for chemical analysis of planetary materials, including extraterrestrial minerals. Its use has helped to identify several from the Earth yet unknown phases, including also niningerite. EPMA has many advantages, including being non-destructive, being conducted on minerals in situ on a micron scale, and being obtained in a relatively short time (McGee and Keil 2001). However, it also has requirements, such as being conducted on a flat, well-polished surface, using well-defined standards for all elements planned to be measured, and for correct analysis, relatively complex matrix correction has to be applied. All matrix corrections in the microprobe software supplied by the manufacturer include correction terms for atomic number (Z), absorption (A), and fluorescence (F). For the scope of this article, it is necessary to explain the fluorescence in more detail. Fluorescence is the phenomenon in which the emission of the characteristic X-ray can be excited by another characteristic X-ray due to the latter exceeding the critical excitation energy of the former. One of the well-known examples is the Fe $K\alpha$ (6.40 keV) excitation of Cr $K\alpha$ (critical excitation energy 5.99 keV). Considering this scenario, chromium concentration would have been incorrectly increased without applying the fluorescence correction (Reed 2005). More importantly, a phenomenon called boundary fluorescence still might be an issue since it is not corrected in EPMA software supplied by the manufacturer. To our knowledge, the commercial third-party software called Probe for EPMA (Donovan et al. 2012), however, does allow for simulating the effect. Boundary fluorescence occurs when the whole analytical volume of the sample is not homogenous. Consequently, the inclusion of a phase that contains a sufficiently high concentration of an element that may be excited by an element significantly present in the main mass may cause a considerable contribution to the apparent chemical composition of the main mass (Reed 2005).

In the earth sciences, accelerating voltages used traditionally for EPMA analysis of silicates or oxides are 15 kV, whereas for sulfides, 20 kV (Sweatman and Long 1969). At the same time, the accelerating voltage affects the analytical volume substantially. When measuring small inclusions, lamellas, or fine-grained materials, it is

desirable to excite the smallest possible analytical volume. This helps to reduce or completely suppress the potential contribution from the surrounding material. The development and integration of the Schottky field emission guns (FEG) as an electron source for EPMA (FEG-EPMA) contributed significantly to the matter. In recent years, FEG-EPMA has gained many additional advantages, including the possibility of performing an analysis using low accelerating voltage (5–7 kV) measuring the elements like iron on L-series lines ($L\alpha$, $L\beta$ or L1 line) with finely focused electron beam and relatively high (up to 100 nA) probe currents (McGee and Keil 2001; Rinaldi and Llovet 2015; Moy et al. 2022). However, the FEG-EPMA instruments are not as widely available as the traditional EPMA employing a tungsten filament or solid-state hexaboride crystals (LaB₆ or CeB₆) electron source. Unfortunately, the low accelerating voltage (low-kV) approach is not suitable for EPMAs employing electron sources other than FEG, either due to low brightness of an electron beam (electron density of the electron source), as in the case of tungsten filament, or low stability over a long period of time, as in the case of LaB₆ electron source. For the reduction of analytical volume employing tungsten filament or LaB source, it is possible to implement an analytical procedure called the low-overvoltage (low-U) approach (McSwiggen 2014). Typically, for routine analysis, it is recommended that an accelerating voltage be used to excite the characteristic X-rays that is twice as high as the critical ionization energy (overvoltage) of measured elements. The low-U approach reduces the accelerating voltage to the minimum required to produce the characteristic $K\alpha$ X-ray for some of the elements to be measured (typically transition metals). This decreases the analytical volume from which the characteristic X-rays are generated and escaping from the sample. Both approaches have their advantages and disadvantages (McSwiggen 2014). It is beyond the scope of this article to examine them closely.

This study compares the chemical composition of the sulfides from the enstatite-rich meteorites as measured with a conventional EPMA using 20 kV accelerating voltage with that measured using the low-U approach with 10 kV accelerating voltage to assess the effect of the analytical volume reduction.

2. Material and methods

We analyzed the set of one-inch polished thick sections of enstatite-rich meteorites consisting of nine enstatite chondrites and one aubrite loaned from the collection of the National Institute of the Polar Research (NIPR) in Tokyo, Japan, and the aubrite Mayo Belwa from the collection of the Institute of Geology of the Czech Academy of Sciences in Prague. The samples loaned from NIPR

(the abbreviation and classification including the classification proposed by Weyrauch et al. 2018 are given in parentheses) are those collected in Antarctica near the Asuka Station on the Nansen Icefield: Asuka 881314 (A-881314, EL_a3), Asuka 882067 (A-882067, EL_a3), Asuka 12245 (A-12245, EL_a4), and from the Yamato Mountains: Yamato 691 (Y-691, EH_a3), Yamato 791790 (Y-791790, EH_b3), Yamato 74370 (Y-74370, EH_a4), Yamato 793225 (Y-793225, EH6-an/Ean), Yamato 82189 (Y-82189, EH-imp melt/EH_a), Yamato 86004 (Y-86004, EH-imp melt/EH_b), Yamato 793592 (Y-793592, aubrite).

All samples were carbon-coated for scanning electron microscopy (SEM) and EPMA. The chemical composition of sulfides was obtained with a JEOL 8230 Superprobe equipped with a LaB6 electron source, five wave-length dispersive crystal spectrometers (WDS), and an energydispersive spectrometer (EDS) housed at the Institute of Geology of the Czech Academy of Sciences in Prague. The first set of analyses was measured with the following analytical conditions: an accelerating voltage of 20 kV, 4 nA probe current, and a focused beam. The second set of analyses was measured with an accelerating voltage of 10 kV, 25 nA probe current, and 1 µm beam diameter. For imaging with a 10 kV accelerating voltage, probe currents of 1 nA or less were used to enhance the image resolution. The analyzed elements (used spectral lines, standards, spectrometer crystal, and average detection limits (3 σ) in ppm are listed in parentheses) include Mg ($K\alpha$, magnesium metal, TAPL, 100), Si (Kα, pure silicon, TAPL, 180), P (Kα, synthetic InP, PET, 770), S (Kα, marcasite, PET, 750), Ca (Kα, synthetic CaF₂, PETL, 190), Ti (Kα, titanium metal, PETL, 290), Cr (Kα, chromium metal, LIFH, 430), Mn $(K\alpha, \text{ manganese metal, LIFH, 450})$, Fe $(K\alpha, \text{ marcasite, LIF,})$ 1950), Co ($K\alpha$, cobalt metal, LIF, 1120), Ni ($K\alpha$, nickel metal, LIF, 1900), Cu (Kα, copper metal, LIFH, 410), Zn ($K\alpha$, sphalerite, LIFH, 530). The same spectral lines and analytical crystals were used for analysis employing the 10 kV accelerating voltage except those for cobalt, copper, and zinc [Co ($L\alpha$, TAPL), Cu ($L\alpha$, TAPL), and Zn ($L\alpha$, TAPL)]. Also, the detection limits (3 σ) are different from those obtained using 20 kV accelerating voltage: Mg (80 ppm), Si (120 ppm), P (140 ppm), S (330 ppm), Ca (210 ppm), Ti (380 ppm), Cr (860 ppm), Mn (1030 ppm), Fe (3300 ppm), Co (900 ppm), Ni (6800 ppm), Cu (270 ppm), Zn (200 ppm). Samples Y-791790, Y-74370, A-882067, and Mayo Belwa displayed low totals when measured using 20 kV, and it was assumed that either they contained djerfisherite (K₆Na(Fe,Cu,Ni)₂₅S₂₆Cl) or some mineral with inherited compositional deficit. Consequently, they were analyzed with settings extended by Na ($K\alpha$, jadeite, TAPL, 430 ppm), Cl (Ka, RbCl, PETH, 160 ppm), K (Ka, leucite, PETL, 220 ppm). For further consideration, only the analyses with totals in the range from 98 to 101 % were taken into account. The troilite and (Mg,Fe,Mn)S-monosulfide formulas were recast based on 2 atoms per formula unit. The daubréelite formula calculation was based on 7 atoms per formula unit.

The back-scattered electron (BSE) images were obtained using the scanning electron microscope (SEM) Tescan Vega 3 XMU equipped with Oxford Instruments Ultim Max 65 EDS housed at the Institute of Geology of the Czech Academy of Sciences. Various accelerating voltages and absorbed currents were used to achieve the best possible resolution of the images. High-resolution images were obtained using the SEM with FEG electron source (FEG-SEM) FEI Quanta 200F housed at the Department of Physics of Materials,

Faculty of Mathematics and Physics, Charles University in Prague, using 8 kV to 15 kV accelerating voltages.

3. Results

3.1. Troilite and troilite—daubréelite relationship

Table 1 shows the average chemical composition of troilites, and Tab. 2 shows the average composition of

Table 1. The average chemical composition of trolites of the enstatite-rich meteorites acquired by EPMA using 10 and 20 kV accelerating voltage (in wt. %) and their calculated empirical formulas (in apfu).

			Y-79	91790		Y-74370						
troilite	10 kV		20 kV		10 kV		20 kV		10 kV		20	kV
n	45	σ	27	σ	21	σ	31	σ	15	σ	42	σ
S	36.48	0.16	36.93	0.67	36.94	0.31	37.13	0.34	36.70	0.23	36.69	0.39
Ti	0.28	0.05	0.29	0.05	0.30	0.02	0.30	0.02	0.35	0.07	0.35	0.05
Cr	1.18	0.21	1.33	0.36	1.91	0.11	1.86	0.04	0.46	0.16	0.43	0.09
Mn	0.10	_	0.06	0.01	0.25	0.07	0.25	0.05	0.17	0.00	0.07	0.04
Fe	61.82	0.63	61.29	0.83	60.30	0.63	59.80	0.53	62.19	0.73	61.14	0.63
Co	0.16	0.04	0.15	0.03	0.32	0.24	0.18	0.02	0.27	0.08	0.13	0.02
Cu	0.04	0.02	0.07	0.02	0.08	0.02	0.06	0.01	0.04	0.01	0.06	0.01
Total	99.84	0.57	100.12	0.64	100.18	0.51	99.51	0.61	100.12	0.56	98.91	0.49
S	1.000	0.005	1.007	0.014	1.006	0.006	1.016	0.006	1.003	0.006	1.012	0.007
Ti	0.005	0.001	0.005	0.001	0.005	0.000	0.005	0.000	0.006	0.002	0.007	0.001
Cr	0.020	0.003	0.022	0.006	0.032	0.002	0.031	0.001	0.008	0.003	0.007	0.001
Mn	< 0.001	_	< 0.001	_	0.004	0.002	0.004	0.001	< 0.001	_	< 0.001	-
Fe	0.973	0.007	0.960	0.013	0.943	0.010	0.939	0.001	0.976	0.010	0.969	0.009
Co	0.002	0.001	< 0.001	_	0.004	0.004	< 0.001	_	0.004	0.001	< 0.001	_
atoms	2.000		2.000		2.000		2.000		2.000		2.000	
cations	0.999	0.005	0.991	0.011	0.992	0.006	0.983	0.006	0.996	0.007	0.987	0.007
anions	1.001	0.005	1.009	0.011	1.008	0.006	1.017	0.006	1.004	0.007	1.013	0.007
an/cat	1.001	0.010	1.018	0.022	1.016	0.013	1.034	0.012	1.008	0.013	1.027	0.015
		Y-79322					2189		Y-86004			
troilite		kV		kV		kV		kV		kV		kV
n	25	σ	19	σ	29	σ	40	σ	42	σ	19	σ
S	36.63	0.35	36.80	0.23	36.64	0.54	36.97	0.30	36.32	0.33	37.09	0.32
Ti	1.22	0.63	0.85	0.17	0.21	0.12	0.37	0.12	0.33	0.03	0.33	0.01
Cr	0.86	0.50	0.79	0.19	1.49	0.35	1.61	0.42	1.92	0.17	1.95	0.07
Mn	0.29	0.30	0.05	0.01	0.11	0.01	0.06	0.02	0.25	0.05	0.26	0.05
Fe	60.69	1.09	60.32	0.52	60.85	0.98	60.72	0.70	60.53	0.63	60.16	0.70
Co	0.16	0.04	0.12	0.01	0.28	0.09	0.21	0.04	0.18	0.04	0.14	0.02
Cu	0.07	0.04	0.06	0.01	0.08	0.04	0.02	0.01	0.04	0.02	0.05	0.01
Total	99.59	0.52	98.85	0.44	99.55	0.76	99.80	0.61	99.60	0.66	99.98	0.59
S	1.004	0.007	1.014	0.005	1.006	0.012	1.011	0.006	0.997	0.007	1.011	0.007
Ti	0.021	0.013	0.016	0.003	0.003	0.002	0.007	0.002	0.006	0.001	0.006	0.000
Cr	0.015	0.008	0.013	0.003	0.025	0.006	0.027	0.007	0.033	0.003	0.033	0.001
Mn	< 0.001	_	< 0.001	-	< 0.001	_	< 0.001	_	0.004	0.001	0.004	0.001
Fe	0.956	0.018	0.955	0.007	0.959	0.014	0.953	0.011	0.954	0.008	0.941	0.011
Со	0.002	0.001	< 0.001	_	0.004	0.002	< 0.001	_	0.002	0.001	< 0.001	_
atoms	2.000		2.000		2.000		2.000		2.000		2.000	
cations	0.996	0.007	0.985	0.005	0.993	0.011	0.989	0.006	1.002	0.008	0.989	0.007
anions	1.004	0.007	1.015	0.005	1.007	0.011	1.011	0.006	0.998	0.008	1.011	0.007
an/cat	1.009	0.014	1.030	0.011	1.014	0.024	1.023	0.012	0.997	0.015	1.022	0.014

daubréelites (if present) and their calculated empirical formulas for both accelerating voltages. Figure 1 compares the results between both accelerating voltages. The complete data set of the chemical composition of troilite and daubréelite for both accelerating voltages and corresponding empirical formulas is published by Mészárosová (2024). To gain a clearer spatial understanding of the relationship between troilite and daubréelite, refer to Electronic Supplementary Material (ESM 1). The results below are divided into sections relating to enstatite chondrites and aubrites.

3.1.1. Enstatite chondrites

In Y-86004 and Y-791790, no daubréelite was found even during the high-magnification FEG-SEM study and supplementary TEM study, from which the results will be presented elsewhere. The chemical compositions of troilites in these samples were similar, with relatively high contents of Cr (\sim 2 wt. %) and some trace enrichment in Mn (\sim 0.3 wt. %) and Mg (\sim 0.03 wt. %), although part of the magnesium may represent an artifact due to surroundings, especially when coupled with the presence

Table 1. Continued

			81314				82067		A-12245						
troilite	10	10 kV		20 kV		10 kV		20 kV		kV	20	kV			
n	17	σ	34	σ	14	σ	32	σ	71	σ	27	σ			
S	36.06	0.39	36.70	0.25	36.90	0.21	37.18	0.27	36.86	0.54	36.97	0.50			
Ti	0.51	0.11	0.52	0.02	0.48	0.09	0.43	0.13	0.60	0.32	0.56	0.28			
Cr	0.45	0.14	0.49	0.10	0.50	0.13	0.53	0.22	2.58	3.91	1.92	3.95			
Mn	0.56	0.45	0.05	0.00	0.27	0.14	0.10	0.07	0.76	0.86	0.23	0.24			
Fe	62.59	0.54	61.82	0.46	62.14	0.38	61.78	0.57	58.96	5.17	59.04	4.86			
Co	0.15	0.05	0.20	0.03	0.31	0.09	0.12	0.00	0.15	0.05	0.14	0.02			
Cu	0.05	0.02	0.02	0.00	0.04	0.02	0.02	0.00	0.24	0.41	0.07	0.03			
Total	99.87	0.67	99.57	0.53	100.48	0.34	100.01	0.56	100.04	0.56	98.94	0.54			
S	0.991	0.006	1.007	0.005	1.004	0.004	1.014	0.007	1.006	0.010	1.017	0.010			
Ti	0.009	0.002	0.010	0.000	0.009	0.002	0.008	0.002	0.011	0.006	0.010	0.005			
Cr	0.008	0.002	0.008	0.002	0.008	0.002	0.009	0.004	0.043	0.065	0.032	0.066			
Mn	0.002	0.005	< 0.001	_	0.001	0.002	< 0.001	_	0.008	0.013	0.002	0.003			
Fe	0.988	0.008	0.974	0.005	0.971	0.005	0.967	0.007	0.924	0.084	0.933	0.079			
Co	0.002	0.001	< 0.001	_	0.005	0.001	< 0.001	_	0.001	0.001	< 0.001	_			
atoms	2.000		2.000		2.000		2.000		2.000		2.000				
cations	1.009	0.006	0.993	0.005	0.995	0.004	0.985	0.007	0.994	0.011	0.983	0.009			
anions	0.991	0.006	1.007	0.005	1.005	0.004	1.015	0.007	1.006	0.011	1.017	0.009			
an/cat	0.983	0.012	1.015	0.011	1.010	0.008	1.030	0.014	1.012	0.022	1.036	0.020			
		Y-79	93592			Mayo	Belwa								
troilite	10	10 kV		20 kV		kV	20 kV		_						
n	42	σ	33	σ	36	σ	16	σ	-						
S	37.03	0.81	37.71	0.52	36.70	1.22	36.50	0.53							
Ti	3.67	3.41	2.99	2.05	2.58	1.35	2.59	0.65							
Cr	0.57	0.42	0.60	0.54	0.41	0.20	0.40	0.14							
Mn	0.30	0.21	0.14	0.11	0.33	0.53	0.12	0.13							
Fe	57.92	4.36	58.00	3.12	59.36	2.12	58.78	1.24							
Co	0.15	0.06	b.d.l.	_	0.26	0.09	0.14	0.01			e not includ				
Cu	0.06	0.04	0.06	0.02	0.05	0.01	0.05	_		-	were not an	•			
Total	99.28	0.70	99.56	0.69	99.75	0.79	98.58	0.44			on limits (b. numbers o	//			
S	1.012	0.014	1.025	0.010	1.001	0.026	1.007	0.011	1		taset for th	-			
Ti	0.063	0.061	0.054	0.037	0.047	0.025	0.048	0.012	lar minera		itaset for th	e partieu			
Cr	0.010	0.007	0.010	0.009	0.007	0.003	0.007	0.002							
Mn	0.001	0.003	< 0.001	_	0.003	0.007	0.001	0.002							
Fe	0.910	0.075	0.905	0.052	0.930	0.034	0.931	0.021							
Co	0.001	0.001	_	_	0.003	0.002	< 0.001	_							
atoms	2.000	,	2.000		2.000		2.000		_						
cations	0.987	0.014	0.973	0.011	0.995	0.022	0.990	0.012	_						
anions	1.013	0.014	1.027	0.011	1.005	0.022	1.010	0.012							
an/cat	1.027	0.029	1.056	0.022	1.012	0.041	1.020	0.024							

Table 2. The average chemical composition of daubréelite of the enstatite-rich meteorites in (wt. %) and their calculated empirical formulas (in *apfu*). They were acquired by EPMA using 10 and 20 kV accelerating voltage.

	Y-691 10 kV			Y-7	74370			Y-7	93225		Y-82189			
daubréelite			10 kV		20 kV		10 kV		20 kV		10 kV		20	kV
n		2	13	σ	16	σ	14	σ	13	σ	10	σ	3	σ
Mg	0.02	0.01	0.06	0.09	0.02	0.01	0.01	0.01	0.02	0.01	0.03	0.01	0.02	0.00
S	43.66	43.55	43.83	0.29	44.30	0.34	43.64	0.27	44.33	0.37	43.40	0.84	44.13	0.24
Ti	0.14	0.18	0.11	0.03	0.04	0.01	0.09	0.03	0.08	0.02	0.24	0.13	0.23	0.08
Cr	34.59	34.68	35.02	0.37	35.38	0.27	36.20	0.40	35.54	0.24	34.39	1.29	34.63	0.20
Mn	1.05	1.07	0.63	0.22	0.55	0.06	1.76	0.52	1.86	0.53	0.55	0.21	0.32	0.04
Fe	17.63	18.84	17.37	1.03	16.00	0.56	17.65	0.59	17.17	0.56	19.20	1.89	17.84	1.03
Co	b.d.l.	0.12	0.27	0.06	b.d.l.	_	0.10	0.00	0.12	0.00	0.24	0.09	0.18	0.00
Ni	b.d.l.	b.d.l.	b.d.l.	_	0.80	0.26	b.d.l.	_	b.d.l.	_	b.d.l.	_	b.d.l.	_
Cu	0.18	0.24	0.12	0.06	0.09	0.02	0.12	0.02	0.11	0.03	0.35	0.18	0.38	0.10
Zn	1.80	0.83	2.27	1.00	2.74	0.48	b.d.l.	_	b.d.l.	_	0.78	0.79	1.39	1.31
Total	99.11	99.51	99.15	0.49	99.28	0.50	99.50	0.54	99.10	0.61	99.12	0.61	98.55	0.03
Mg	0.002	0.002	0.003	0.008	0.001	0.001	0.001	0.001	0.001	0.001	0.002	0.002	0.002	0.000
S	3.976	3.954	3.985	0.012	4.019	0.018	3.952	0.021	4.014	0.011	3.954	0.044	4.023	0.010
Ti	0.009	0.011	0.003	0.004	0.001	0.001	0.006	0.002	0.004	0.002	0.013	0.009	0.014	0.005
Cr	1.943	1.942	1.964	0.019	1.980	0.016	2.022	0.020	1.985	0.011	1.932	0.065	1.947	0.006
Mn	0.056	0.057	0.033	0.012	0.029	0.003	0.093	0.027	0.098	0.028	0.027	0.014	0.017	0.002
Fe	0.922	0.982	0.907	0.053	0.834	0.029	0.918	0.031	0.893	0.030	1.005	0.104	0.934	0.051
Co	_	0.006	0.013	0.003	_	_	0.001	0.002	0.000	0.002	0.011	0.005	0.003	0.004
Ni	_	_	_	_	0.010	0.018	_	_	_	_	_	_	_	_
Cu	0.008	0.011	0.005	0.003	0.004	0.001	0.006	0.001	0.005	0.002	0.016	0.008	0.017	0.005
Zn	0.080	0.037	0.078	0.058	0.122	0.021	_	_	_	_	0.035	0.035	0.042	0.056
atoms	7.000	7.000	7.000		7.000		7.000		7.000		7.000		7.000	
		A-8	81314			A-8	82067			A-1	12245		Y-79	93592
daubréelite	10) kV	20 kV		10 kV		20 kV		10 kV		20 kV		10 kV	
n	10	σ	15	σ	8	σ	17	σ	15	σ	14	σ	8	σ
Mg	0.01	0.00	0.02	0.01	0.02	0.01	0.03	0.02	0.01	0.01	0.01	0.00	0.04	0.02
S	43.38	0.40	44.28	0.34	43.92	0.14	44.75	0.38	43.63	0.32	44.00	0.45	43.57	0.23
Ti	0.15	0.09	0.08	0.04	0.10	0.03	0.07	0.03	0.08	0.04	0.07	0.03	0.07	0.003
Cr	35.52	0.40	35.00	0.28	35.84	0.49	34.83	0.40	35.69	0.33	35.46	0.63	35.61	0.28
Mn	1.27	0.22	1.24	0.09	1.69	0.21	1.87	0.51	1.59	0.57	1.40	0.11	1.60	0.62
Fe	17.80	0.39	17.65	0.29	17.39	0.39	16.91	1.09	17.01	1.52	16.82	0.56	17.46	1.34
Co	0.10	0.003	b.d.l.	_	0.29	0.07	0.11	0.00	0.12	0.01	b.d.l.	_	0.14	_
Ni	0.84	_	b.d.l.	_	b.d.l.	_	b.d.l.	_	b.d.l.	_	b.d.l.	_	b.d.l.	_
Cu	0.23	0.11	0.16	0.05	0.20	0.14	0.12	0.05	0.16	0.04	0.15	0.04	0.15	0.12
Zn	0.72	0.15	0.71	0.16	0.41	0.31	1.11	1.10	1.15	0.86	1.01	0.29	0.55	0.66
Total	99.20	0.64	99.13	0.42	99.88	0.31	99.11	0.59	99.38	0.45	98.93	0.39	98.93	0.62
Mg	0.000	0.001	0.000	0.001	0.001	0.001	0.002	0.002	0.001	0.001	0.001	0.001	0.002	0.003
S	3.949	0.017	4.014	0.017	3.963	0.014	4.045	0.018	3.961	0.018	4.001	0.030	3.967	0.015
Ti	0.009	0.005	0.004	0.003	0.006	0.002	0.004	0.002	0.005	0.003	0.004	0.002	0.001	0.002
Cr	1.994	0.021	1.957	0.016	1.994	0.027	1.942	0.028	1.999	0.019	1.989	0.042	1.999	0.010
Mn	0.068	0.012	0.066	0.005	0.089	0.011	0.099	0.027	0.084	0.030	0.074	0.006	0.085	0.034
Fe	0.930	0.024	0.919	0.014	0.901	0.021	0.878	0.055	0.887	0.080	0.878	0.028	0.912	0.066
Co	0.001	0.002	_	_	0.014	0.003	0.000	0.001	0.002	0.003	_	_	0.001	0.002
2.71														
Ni	0.004	0.012	_	-	_	_	_	_	-	-	-	_	_	_
N1 Cu		0.012 0.005	- 0.007	- 0.002	- 0.009	0.006	0.005	0.003	0.007	0.002	0.007	0.002	0.007	0.006
	0.004													

Some elements were not included in the table because they were not analyzed, were below detection limits (b.d.l.), or were present in only a few samples across the whole dataset for the particular mineral. The chemical composition of daubréelite was successfully acquired using only the 10 kV accelerating voltage in meteorites Y-691 and Y-793592. No daubréelite was observed in Y-791790, Y-86004, and Mayo Belwa.

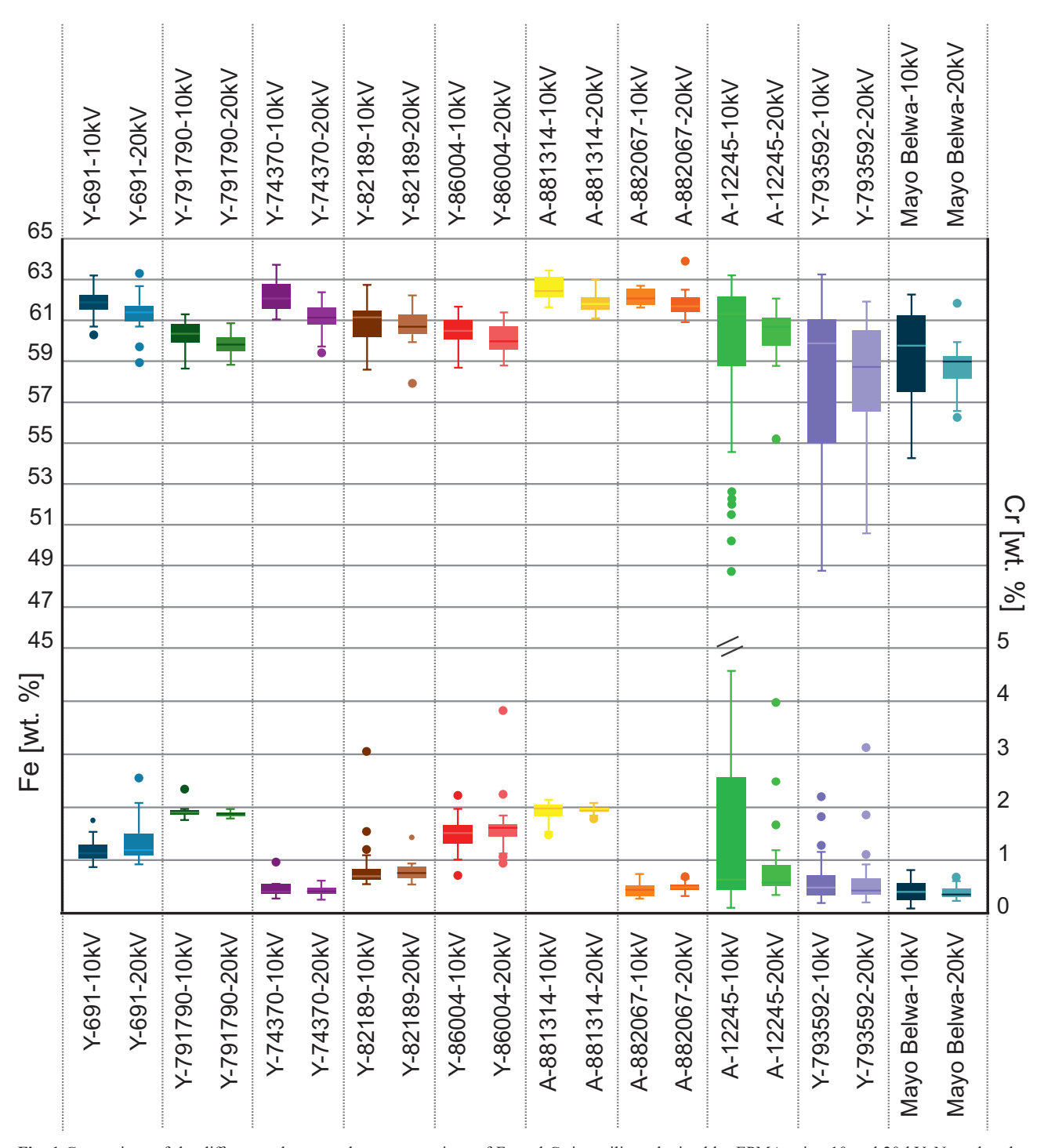


Fig. 1 Comparison of the differences between the concentrations of Fe and Cr in troilites obtained by EPMA using 10 and 20 kV. Note that the high scatter in concentrations of both Fe and Cr in A-12245 results from the complexity of the relationship between troilite, daubréelite, and (Mg,Fe,Mn)S-monosulfide.

of Si. Additionally, trace amounts of Cu and K were occasionally detected in Y-791790.

No visible daubréelite was found using SEM and during EPMA measurement with an accelerating voltage of 20 kV in Y-691. However, the high-magnification FEG-SEM study found fine submicron-sized mutually parallel

lamellas. Besides, a few wider lamellas or inclusions, approximately $1\times 2~\mu m$ in size of daubréelite, were found. Chromium contents in troilite were very variable when measured using 20 kV accelerating voltage. However, even using the 10 kV accelerating voltage did not reduce the variability much. Titanium contents were relatively

low and less variable. Due to the small grain size, only two analyses of daubréelite were obtained with the analytical total in the range of 98–101 wt. %. These grains were enriched in Mn and Zn and trace amounts of Cu.

The remaining samples shared similar troilite composition and troilite-daubréelite relationship with some distinctions. Generally, in A-881314 and Y-74370, daubréelite lamellas emerged from troilite in a variable width ranging from tens to hundreds of microns. No submicron-sized lamellas were observed using high magnification FEG-SEM and low accelerating voltage. However, A-881314 was part of the TEM study (Mészárosová and Skála 2022), and subtle lamellas (~10 nm in width) of daubréelite were confirmed using TEM. Occasionally, daubréelite formed a discrete grain adjacent to troilite. The chemical composition of troilites in these samples was also very similar, with relatively low Cr and Ti contents. In addition to the previously described assemblage, some discrete grains of daubréelite with no adjacent grain of troilite were found in A-882067. However, the troilite grain may be just below the plane imaged by the BSE. The chemical composition was similar to that of previous samples, with relatively low Cr and Ti contents. However, using 20 kV accelerating voltage, some troilite analyses showed elevated Cr contents (~1 wt. % Cr). No analyses with elevated Cr content were observed during the measurement with the 10 kV accelerating voltage. In addition to Cr and Ti, a relatively invariant content of a trace amount of Co was measured in troilites of A-882067 due to lower detection limits using the Co La line (0.3 wt. % Co). Within the daubréelite lamellas in Y-82189, some dark lamellas or parts appeared, possibly due to weathering, or it could be a different Cr-rich mineral (they might represent the Na-Cr hydrated phases reported by El Goresy et al. (1988) but to confirm their presence, a detailed study of these phases would be required). The chemical composition of troilite showed a higher Cr concentration (~1.5 wt. %) than Ti concentration (~0.3 wt. %). Further, some Co enrichment was detected using both accelerating voltages (~0.25 wt. %). The chemical composition of daubréelite, in addition to common Mn enrichment (~0.4 wt. %), occasionally showed some elevated Zn concentrations (~1 wt. %). Also, elevated concentrations of Co and Ti were detected. Daubréelite appeared as very wide, well-defined lamellas in A-12245; however, the complexity of the daubréelite-troilite grains boundary was found using high magnification and low accelerating voltage. Daubréelite itself contained tiny Fe-rich rounded inclusions or irregular lamellas (probably Fe-metal or schreibersite) and submicron-sized dark inclusions or irregular lamellas of probably Cr-rich unknown mineral/s. On the daubréelite-troilite grain boundary, very fine lamellas of daubréelite and troilite alternated, occasionally accompanied by Fe-rich blebs. Those blebs

were rarely included in the troilite part of the assemblage in close proximity to the daubréelite-troilite boundary. Occasionally, (Mg,Fe,Mn)S-monosulfide had a similar appearance as daubréelite, and it was difficult to distinguish them without chemical analysis. In some cases, it was complicated to distinguish the boundary between troilite and daubréelite or (Mg,Fe,Mn)S-monosulfide.

3.1.2. Aubrites

No daubréelite, neither grains nor lamellas, was observed in Mayo Belwa during both searches. A few Cr-rich grains were found and measured; however, their composition did not match daubréelite, and their analytical totals (about 80-85 wt. %) were below the acceptable range (they might represent the Na-Cr hydrated phases reported by El Goresy et al. (1988) as in the case above). No other elements were found during the careful EDS measurement of these grains. The chemical composition of troilite was found to be highly variable (especially in Ti concentration, which varied from 0.5 to ~ 5 wt. %). The amount of Cr was lower but also variable. Some enrichment in other elements, such as Si, K, Ca, Mn, and Co, was detected. In addition to the previously mentioned sulfides, grains of djerfisherite were commonly found. They were adjacent to (Mg,Fe,Mn)S-monosulfide and occurred as irregular grains with a maximum size of 20 μm. Daubréelite adjacent to troilite was observed only occasionally using 20 kV SEM and EPMA in Y-793592. The high magnification observation at low accelerating voltage revealed more daubréelite lamellas and rarely euhedral inclusions in troilites. In some cases, their larger size allowed for acquiring an unbiased composition. The daubréelite was enriched in Mn and occasionally in Zn. Other enrichment (including Ti) could be caused by surrounding contamination due to the small size of lamellas or inclusions. Moreover, in troilites, fine submicroscopic lamellas or round, irregular, micron-sized wavy inclusions of Ti-rich mineral/s were observed. The chemical composition of troilite was found to be variable, even more than in Mayo Belwa, with Ti concentrations varying from ~ 0.05 wt. % to as high as ~ 16 wt. %. Chromium concentration was also more variable than in the troilites of Mayo Belwa, ranging from 0.2 wt. % to 2 wt. %.

3.2. (Mg,Fe,Mn)S-monosulfide and its relationship to troilite—daubréelite

In enstatite chondrites, the occurrence of (Mg,Fe,Mn) S-monosulfide correlates with its chemical composition, and several groups can be recognized, as illustrated in Tab. 3 and Fig. 2. As expected, the chemical composition of (Mg,Fe,Mn)S-monosulfide in aubrites corresponds to alabandite. The complete dataset of the

Table 3. The average chemical composition of (Mg,Fe,Mn)S-monosulfide of the enstatite-rich meteorites (in wt. %) and their calculated empirical formulas (in *apfu*). They were acquired by EPMA using 10 and 20 kV accelerating voltage.

		Y-6	591			Y-79	1790		Y-74370				
(Mg,Fe,Mn)S	10	kV	20 1	kV	10 kV		20 kV		10 1	kV	20	kV	
n	19	σ	19	σ	12	σ	9	σ	20	σ		2	
Mg	29.75	0.65	28.29	0.56	11.36	1.00	10.00	0.55	28.64	0.67	24.87	26.96	
S	50.09	0.62	51.57	0.58	42.49	0.43	42.67	0.43	49.06	0.54	50.14	49.67	
Ca	0.36	0.03	0.41	0.05	1.52	0.06	1.66	0.07	0.21	0.03	0.28	0.26	
Cr	0.16	0.07	0.18	0.08	1.80	0.06	1.76	0.04	0.10	0.02	0.12	0.09	
Mn	5.50	0.38	5.61	0.21	5.11	0.45	4.85	0.18	10.05	0.85	9.36	9.49	
Fe	13.81	0.95	13.55	0.86	36.40	2.12	37.34	1.00	11.07	1.26	13.58	12.18	
Co	0.12	0.02	b.d.l.		0.28	0.08	b.d.1.	_	0.20	0.06	b.d.l.	b.d.l.	
Zn	b.d.l.	_	b.d.l.	_	0.15	0.05	0.19	0.03	0.02	_	b.d.l.	b.d.l.	
Total	99.75	0.75	99.76	0.64	99.98	0.42	98.57	0.50	99.53	0.65	98.35	98.71	
Mg	0.778	0.014	0.743	0.011	0.352	0.028	0.319	0.015	0.759	0.014	0.680	0.725	
s	0.993	0.007	1.026	0.008	1.000	0.005	1.032	0.004	0.985	0.008	1.039	1.013	
Ca	0.006	0.000	0.007	0.001	0.029	0.001	0.032	0.001	0.003	0.000	0.005	0.004	
Cr	0.002	0.001	0.002	0.001	0.026	0.001	0.026	0.000	0.001	0.001	0.001	0.001	
Mn	0.064	0.004	0.065	0.002	0.070	0.006	0.068	0.003	0.118	0.010	0.113	0.113	
Fe	0.157	0.012	0.155	0.010	0.492	0.033	0.518	0.017	0.128	0.015	0.162	0.143	
Co	0.000	0.001	_	_	0.004	0.001	_	_	0.002	0.001	_	_	
Zn	_	_	_	_	0.002	0.001	0.002	0.000	0.000	0.000	_	_	
sum	2.000		2.000		2.000		2.000		2.000		2.000	2.000	
cations	1.006	0.008	0.972	0.008	0.999	0.005	0.967	0.004	1.012	0.007	0.961	0.986	
anions	0.994	0.008	1.028	0.008	1.001	0.005	1.033	0.004	0.988	0.007	1.039	1.014	
an/cat	0.987	0.015	1.057	0.016	1.002	0.010	1.067	0.009	0.976	0.014	1.081	1.029	
	Y-79				Y-82				5004				
(Mg,Fe,Mn)S	10 kV		20 1	kV	10 kV		10 kV		20 1	kV			
n	19	σ	12	σ	8	σ	21	σ	17	σ			
Mg	17.72	1.41	17.18	1.80	24.61	0.91	10.61	0.79	9.69	0.22			
S	45.21	0.83	45.59	0.83	47.36	0.61	41.91	0.49	42.41	0.33			
Ca	0.52	0.13	0.60	0.23	0.54	0.04	1.65	0.02	1.82	0.02			
Cr	0.18	0.04	0.23	0.11	0.47	0.07	1.80	0.06	1.74	0.04			
Mn	20.13	4.34	20.29	5.17	8.34	0.26	3.90	0.23	3.71	0.14			
Fe	16.15	2.21	14.85	2.58	18.21	1.08	38.32	1.34	38.82	0.57			
Co	0.15	_	b.d.l.	_	0.20	0.05	0.14	0.03	0.12	0.01			
Zn	0.02	0.004	b.d.l.	_	0.03	0.01	0.23	0.07	0.29	0.06			
TOTAL	99.92	0.58	98.77	0.49	99.82	0.77	98.58	0.60	98.59	0.44			
Mg	0.518	0.035	0.507	0.046	0.675	0.018	0.338	0.021	0.310	0.007			
S	1.003	0.004	1.021	0.005	0.986	0.007	1.012	0.005	1.029	0.006			
Ca	0.009	0.002	0.011	0.004	0.009	0.001	0.032	0.000	0.035	0.000			
Cr	0.002	0.001	0.003	0.002	0.006	0.001	0.027	0.001	0.026	0.001			
Mn	0.262	0.062	0.266	0.074	0.101	0.003	0.055	0.003	0.053	0.002			
Fe	0.205	0.027	0.191	0.032	0.218	0.014	0.531	0.023	0.541	0.008			
Co	0.000	0.000	_	_	0.002	0.001	0.001	0.001	0.000	0.001			
Zn	0.000	0.000	_	_	0.000	0.000	0.003	0.001	0.003	0.001			
sum	2.000		2.000		2.000	· · · · · · · · · · · · · · · · · · ·	2.000		2.000				
cations	0.997	0.004	0.978	0.005	1.012	0.007	0.988	0.005	0.970	0.006			
anions	1.003	0.004	1.022	0.005	0.988	0.007	1.012	0.005	1.030	0.006			
am/aat	1.000	0.000	1.045	0.000	0.27	0.007	1.025	0.000	1.063	0.000			

chemical composition of (Mg,Fe,Mn)S-monosulfide for both accelerating voltages and corresponding empirical formulas is published by Mészárosová (2024). To better understand the spatial relationship between troilite-daubréelite and (Mg,Fe,Mn)S-monosulfide, see ESM 2.

0.008

1.045

0.010

0.977

0.013

1.006

an/cat

3.2.1. Enstatite chondrites

0.009

1.025

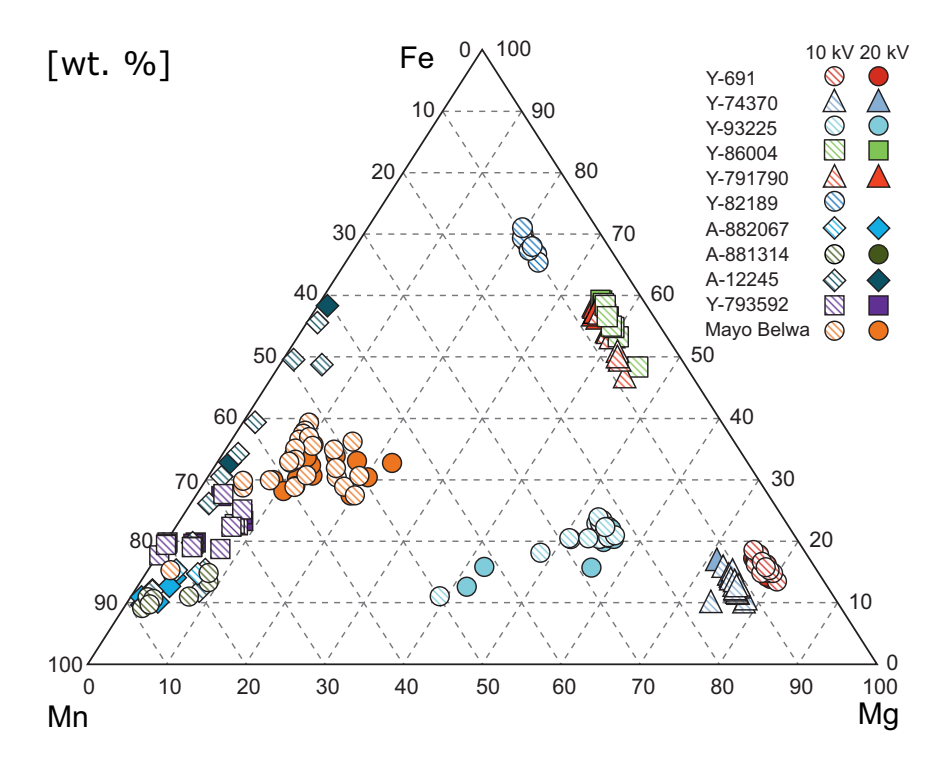
Keilite was present in Y-86004 and Y-791790. In Y-86004, keilite occurred in the form of irregular grains, with troilite appearing on the edges of these grains. Except for the elements usually found in (Mg,Fe,Mn)

1.062

0.012

S-monosulfide, a relatively high concentration of Cr was measured. The chromium content was similar to that in troilites in this sample. In Y-791790, the keilite occurred in close proximity to the troilite or rudashevskyite (cubic (Fe,Zn)S) grains exsolved from troilites. Occasionally, rounded fine inclusions of schreibersite occurred in the keilite grains.

The niningerite was present in EH meteorites Y-691, Y-74370, and Y-82189. In Y-691, niningerite occurred in contact with troilite in rounded sulfide Fe-Ni-metal aggregates or as solitary grains near other sulfides or Fe-Ni-metal. Occasionally, rounded inclusions very bright in BSE (probably schreibersite; not analyzable, but the presence of phosphorous confirmed by EDS) were found in niningerites. Rarely Fe-rich lamellas (presumably troilite) were exsolved from niningerites. The chemical composition of niningerite was slightly enriched in Ca and Cr. In Y-74370, the niningerite appearance was similar to the one described in Y-691, but neither rounded inclusions nor lamellas were found. Only two analyses of niningerite using 20 kV were in the range of 98-101 wt. % in total. Using 10 kV, trace amounts of Na, K, and occasionally Cl were measured in addition to small Ca and Cr enrichment (similar to Y-691), the latter two being observed in both accelerating voltages. In Y-82189, the appearance of niningerite was very similar to that in Y-74370. Unfortunately, no chemical analysis of niningerite was performed using 20 kV because it was difficult to find their grains. They are small and their BSE signal intensity is similar to Fe oxide, which is quite common in this sample (perhaps due to terrestrial weathering).



Niningerite should have been present in Y-793225. However, the composition of (Mg,Fe,Mn)S-monosulfide was variable, showing the intermediate composition between niningerite, keilite, and alabandite (Fig. 2). In addition to Fe, Mg, and Mn, the niningerite contained small amounts of Ca and Cr, similar to the previously mentioned niningerites.

As expected, the alabandite was present in A-881314, A-882067, and A-12245. In A-882067, alabandite was found either as a solitary grain or, more often, in contact with troilite or daubréelite. The chemical composition is relatively homogeneous. This meteorite was measured using the extended setting, so some potassium was measured in alabandite. Also, some elevated Co content was found. One alabandite grain showing elevated Fe content was found in A-881314, next to those displaying features described for this mineral occurring in A-882067. However, this could be due to small (less than 1 µm) ellipsoidal inclusions of Fe-rich mineral (probably troilite) found in that particular grain. Otherwise, the chemical composition is relatively homogeneous. In A-12245, alabandite was found rarely. If it was present, it was usually part of the troilite-daubréelite assemblage with diffuse edges or extremely fine troilite lamellas alternating with the alabandite. The chemical composition of the alabandite was found to be heterogeneous. However, it could be due to the small size of the grains, which could cause the subsequent bias of the analysis from the surrounding troilite or daubréelite. One grain really stood out with its composition closer to the keilite end-member instead of alabandite; however, this particular grain contained irregular laminar inclusions of a phase brighter in BSE (prob-

> ably troilite), so they could have also caused the iron enrichment.

3.2.2. Aubrites

The chemical composition of the (Mg,Fe,Mn)S-monosulfide was found to be quite heterogeneous in Mayo Belwa. It corresponded to alabandite with a slightly increased concentration of Fe. Occasionally, a trace concentration of Cr and rarely Ti was found. However, it could be biased due to the small grain

Fig. 2 Chemical composition of (Mg,Fe,Mn)S-monosulfide in enstatite-rich meteorites obtained by EPMA using 10 and 20 accelerating voltages. Chromium content was added to the iron part of the ternary diagram to present the data as Cr has a higher affinity for iron than the other two elements.

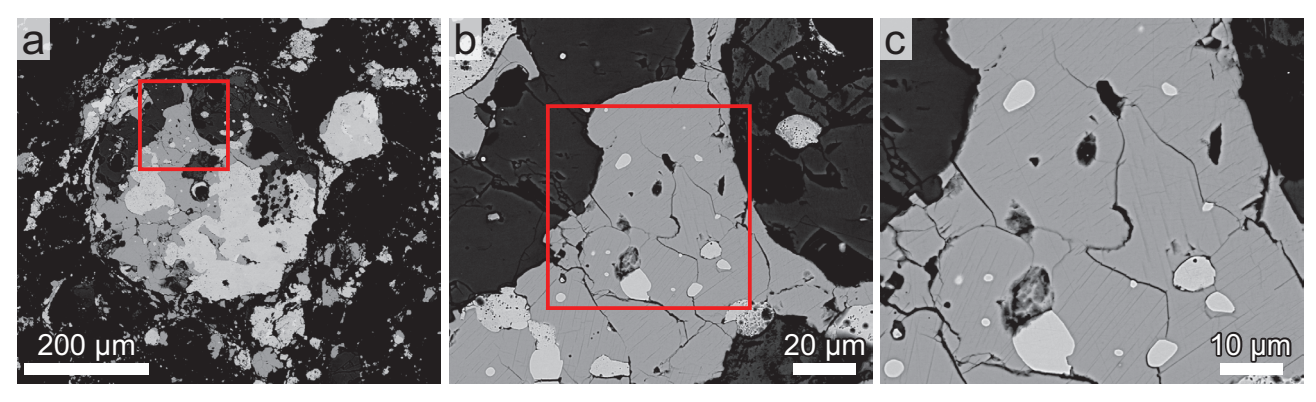


Fig. 3 Troilite grain in Y-691 imaged with various magnifications. Notice that the daubréelite lamellas are clearly visible only when using high magnification.

size and the close proximity of troilite, Fe-Ni-metal, or djerfisherite. In Y-793592, alabandite was also found with increased and fluctuating concentrations of Fe. Otherwise, trace concentrations of Ca and Mg were found. Fluctuation and iron enrichment might be caused by tiny inclusions, as they were observed in one of the grains.

4. Discussion

In general, the presence of daubréelite lamellas in troilites of enstatite-rich meteorites has long been known among members of the meteorite research community. Weyrauch et al. (2018) pointed out that both EH and EL groups can be divided into two subgroups according to whether they contain daubréelite. Determination of the daubréelite presence may be challenging due to the possibility of being present only as tiny lamellas as we had observed in our thick section of Y-691, which is also in agreement with past observations (Ikeda 1989). However, the presence of daubréelite might be crucial to determine the equilibrium temperature for sulfides since, above 700 °C, no daubréelite is present according to the Fe-Cr-S phase diagram (El Goresy and Kullerud 1969). Similarly, the unnoticed tiny Fe-rich inclusions or lamellas in (Mg,Fe,Mn)S-monosulfide might erroneously indicate the Fe enrichment and, therefore, false equilibrium temperature of sulfides. The chemical composition of this phase is considered suitable for determining the equilibrium temperature as the increasing Fe content is coupled with the increasing equilibrium temperature of the system (Skinner and Luce 1971). If the meteorite contains only tiny lamellas of daubréelite, it would not be possible to recognize using large area element mapping. Consequently, without further investigation, the meteorite may be considered not to contain daubréelite. Even when screening the samples visually, it might be difficult to notice the tiny lamellas. Therefore, we want to highlight the importance of magnification when attempting to detect tiny daubréelite lamellas.

As shown in Fig. 3, until the magnification is high enough, it is nearly impossible or highly demanding to see the lamellas. Due to the difficulty of detecting tiny lamellas, a priori knowledge about the possibility of their presence is essential to adjust the procedure for setting the analytical point for EPMA analysis. While selecting the analytical points, the live images are usually noisier and have worse resolution, even if taken at the slowest scanning speed. It is also essential to properly adjust the brightness and contrast of the live images during the measurement setting. Similarly, the brightness and contrast of the BSE images taken can significantly impact the ability to detect tiny lamellas during post-processing and when evaluating the measured data.

Another highly important parameter is the electron density of the electron source (the brightness of the electron source), which can affect the possibility of detecting tiny lamellas. Two assemblages in Y-793592 were imaged using SEM with tungsten filament, EPMA with LaB crystal, and FEG-SEM to demonstrate the effect of different brightness of various electron sources. As shown in Fig. 4, the increasing brightness of the electron source from a tungsten filament through LaB6 to an FEG enables the detection of the lamellas or inclusion more clearly. The diameter of the electron beam plays an important role as well. The FEG is the electron source with the smallest beam diameter over the whole range of beam currents. Similarly, the LaB₆ electron source gives a smaller beam diameter within the entire range of beam currents compared to the tungsten filament, yet its beam still has a larger diameter than that of FEG. Another possibility for enhancing the imaging is decreasing the working distance. Unfortunately, this is impossible with EPMA, as it requires a fixed working distance to maintain geometrical conditions for WDS analyses (Reed 2005).

During our TEM study, the results of which will be published separately, it emerged that although the meteorite contains larger daubréelite lamellas or grains, it simultaneously contains tiny lamellas of daubréelite in troilite. Additionally, EDS measurement conducted dur-

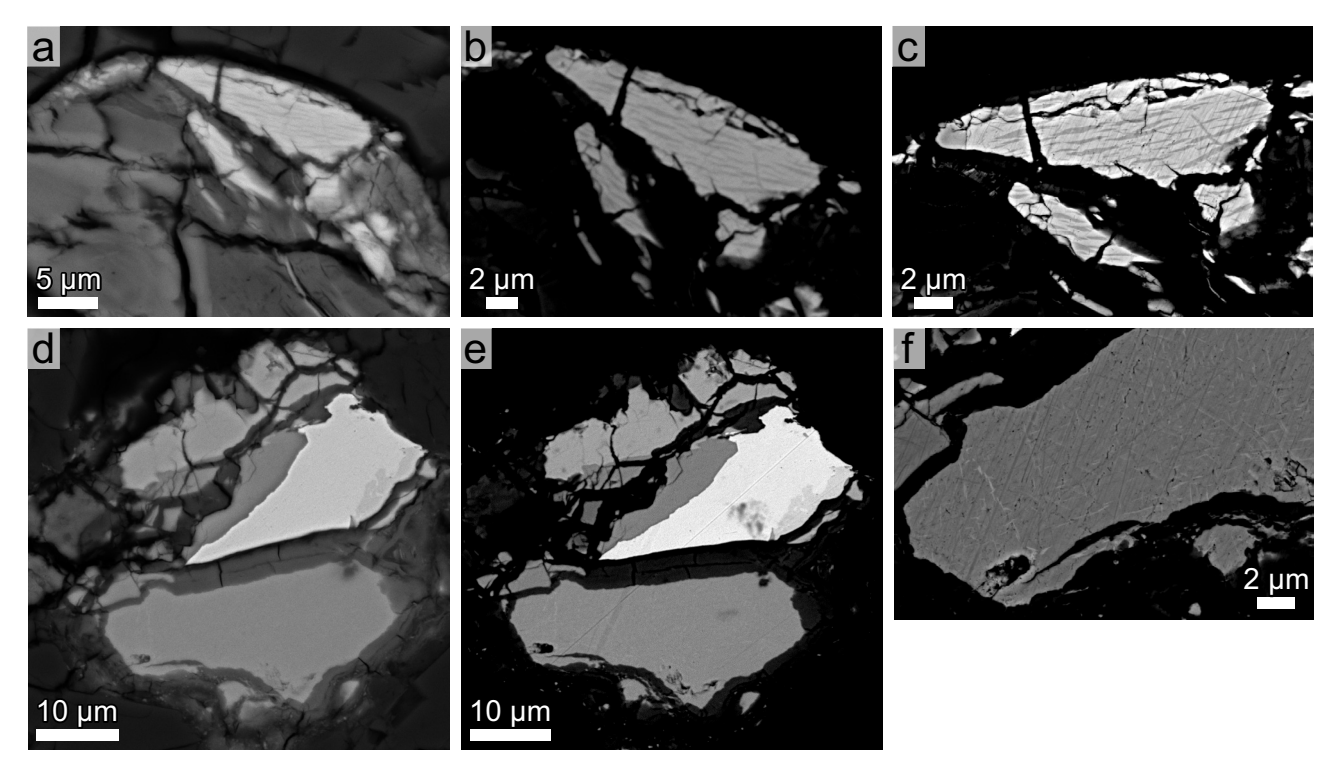


Fig. 4 a-c – Troilite with wavy inclusions of Ti-rich phase in Y-793592 imaged with various instruments and electron sources to demonstrate the difference in brightness of distinct electron sources. \mathbf{a} – SEM equipped with tungsten filament \mathbf{b} – EPMA with LaB₆ crystal \mathbf{c} – FEG-SEM. \mathbf{d} – \mathbf{f} – Sulfide assemblage consisting of troilite, Fe-Ni-metal, and (Mg,Fe,Mn)S-monosulfide in Y-793592. \mathbf{d} – SEM equipped with tungsten filament \mathbf{e} – EPMA with LaB₆ crystal \mathbf{f} – FEG-SEM. Note that the individual panels are slightly rotated relative to each other.

ing the TEM analysis confirmed a trace amount of Cr incorporated in the structure of troilite. We have already observed this in the case of A-881314 (Mészárosová and Skála 2022). Consequently, we expect that it might probably be the case for all the other enstatite-rich meteorites containing large daubréelite grains. Therefore, it is impossible to avoid the contribution of all the lamellas and tiny inclusions to the EPMA results. This influence will always be impossible to quantify. Similarly, the concentration of Mn or Mg in troilite might be influenced by the small inclusions of (Mg,Fe,Mn)S-monosulfide, which were also observed during the TEM study. Nevertheless, we argue that the influence would be smaller with a smaller analytical volume. Therefore, we will compare the results we obtained using 20 and 10 kV accelerating voltages.

Figure 5 shows the difference in the volume of the interaction of the initial electron beam and, therefore, in analytical volumes for 10, 15, and 20 kV simulated by the Monte Carlo approach available in CASINO software (Drouin et al. 2007). With a lower accelerating voltage, a smaller volume of the sample interacts with the initial beam. Therefore, it is also a shallower depth that the characteristics X-ray are generated and escape from the sample. The lower accelerating voltage generates the signals used for imaging (both SE and BSE) from shallower depths and, therefore, have advantages for imag-

ing. However, it also highlights the scratches caused by polishing, as seen in Fig. 6. Therefore, without previous knowledge about the presence of lamellas, they could be mistakenly identified as scratches and vice versa.

Statistically, with a smaller analytical volume, it is less probable to accidentally measure some inclusion or lamella/s at the surface but not seen, or lamella/s below the surface. However, due to the ability of Fe $K\alpha$ to additionally excite Cr $K\alpha$ (boundary fluorescence), the issue is more complicated (Reed 2005). To demonstrate the effectivity of Cr $K\alpha$ to be excited by Fe $K\alpha$, boundary fluorescence was simulated using the FANAL software (Llovet et al. 2012) implemented in the PENEPMA software (Llovet and Salvat 2017). As daubréelite was not an option included in the library for simulation, troilite and FeCr₂S₄ with composition calculated from the formula were chosen to simulate the impact of the boundary fluorescence.

Figure 7 shows the concentration of the simulated amount of "measured" Cr in otherwise Cr-free troilite at various distances from the boundary with the FeCr₂S₄ for 10, 15, and 20 kV accelerating voltages. The amount of Cr detected due to the boundary fluorescence is, in the case of 10 kV, significantly lower than for higher acceleration voltages. However, even when using 10 kV, chromium content is noticeably influenced due to the effect of boundary fluorescence, even at relatively great distances. Clearly, even the 10 kV accelerating voltage

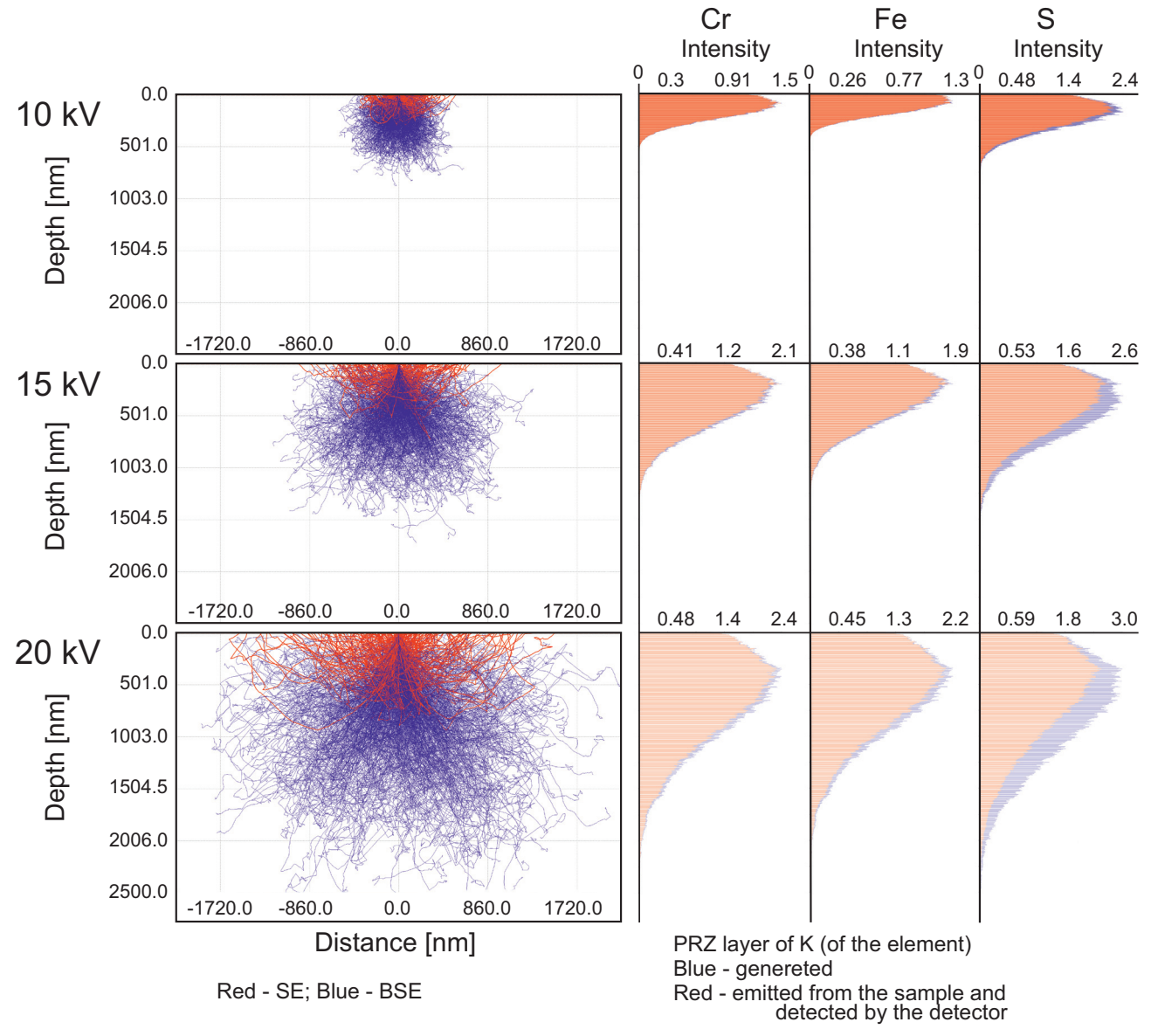


Fig. 5 Interaction of the initial electron beam with the sample of $F_{0.5}Cr_{0.5}S$ composition using accelerating voltages of 10, 15, and 20 kV simulated by the Monte Carlo approach. On the left side of the figure, the difference in the volume and depth of generated SE (red) and BSE (blue) are shown. On the right side, the intensities and the depth from which are $K\alpha$ X-rays of Cr, Fe, and S generated (blue) and emitted and therefore detected (red) for 10, 15, and 20 kV accelerating voltages.

does not mitigate the effect completely. Moreover, the increase in Cr content apparently would be caused not only by the secondary fluorescence but also by the sole presence of the daubréelite lamellas. Fortunately, boundary fluorescence is not an issue for any other element than Cr in present study. The elevated concentration of Mn $K\alpha$ can not be attributed to the boundary fluorescence as the energy of Fe $K\alpha$ is not high enough to excite Mn $K\alpha$ (Mn K edge is 6.538 keV). The element capable of causing boundary fluorescence of Mn $K\alpha$ is Co $K\alpha$ (6.926 keV). However, in enstatite-rich meteorites, phases with a high concentration of Co (main element level of concentration) are not common.

When comparing the analyses carried out with 20 and $10 \, \text{kV}$ accelerating voltages, the average concentrations did not differ significantly (Fig. 1). Interestingly, the Fe content was overall lower for analyses obtained using $20 \, \text{kV}$ accelerating voltages, while the Cr content generally remained the same for both accelerating voltages. A possible explanation for this is that part of the Fe K α was consumed due to the excitation of the Cr K α , which, however, would not be able to escape from the sample and, therefore, was not detected. However, the data for both accelerating voltages were relatively stoichiometric. Nevertheless, the atomic metal-to-sulfur ratio, as shown in Tab. 1, was closer to the ideal (one-to-one) in most cases for analyses acquired

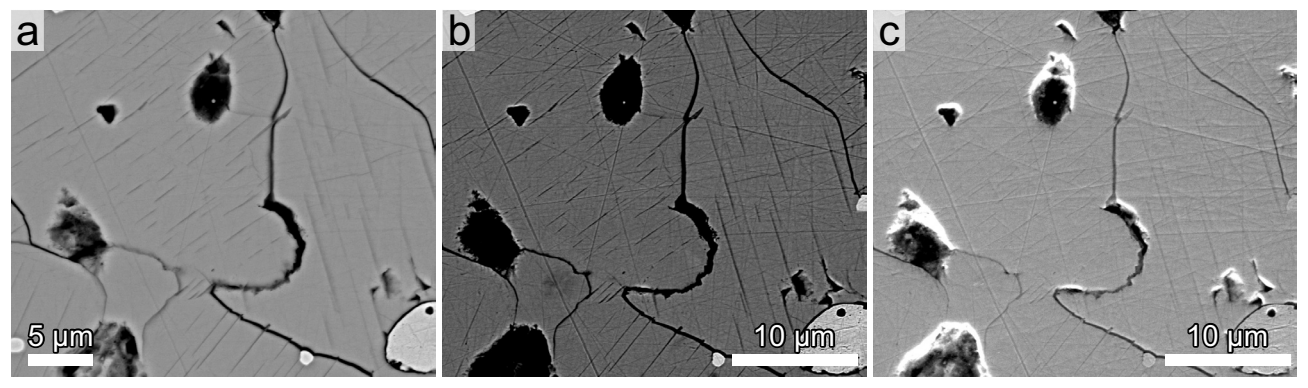


Fig. 6 Troilite with parallel daubréelite lamellas from Y-691 imaged using different accelerating voltages and detectors. a - 15 kV and BSE detector. b - 8 kV and BSE detector. c - 8 kV and SE detector. All images were taken using the same FEG-SEM.

using 10 kV accelerating voltage. In some cases, the extreme values in Cr concentration were measured for both accelerating voltages. With the exception of A-12245 (in which the troilite-daubréelite relationship was found to be very complex), these values are relatively rare.

However, using the 10 kV accelerating voltage introduces some difficulties and disadvantages in the EPMA analysis. When using the 10 kV accelerating voltage, it is essential to have a carbon coat layer of similar thickness otherwise the difference between the thickness of the layer on samples and the standard used for standardization would cause the difference in detected counts (McSwiggen 2014). Further, the results of the analysis are more accurate when both the standard and the measured sample

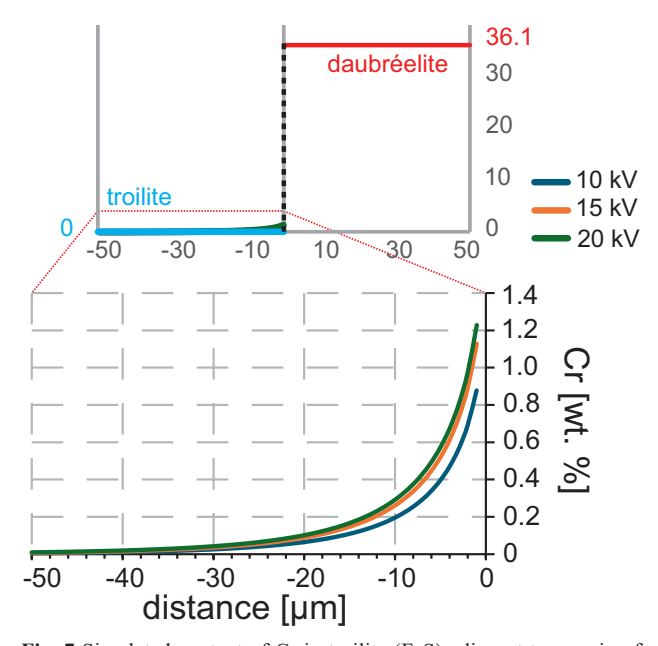


Fig. 7 Simulated content of Cr in troilite (FeS) adjacent to a grain of daubréelite (FeCr $_2$ S $_4$). The shown presence of chromium in nominally Cr-free troilite is due to a boundary fluorescence. The content of Cr is quite high for all simulated accelerating voltages. Nevertheless, the lowest increase in Cr content due to boundary fluorescence is recorded for the accelerating voltage of 10 kV.

contain similar concentrations of the analyte. This issue was illustrated when schreibersite and Fe-Ni-metal were measured with marcasite as a calibration standard during our measurements. The analytical totals of the analyses were significantly higher than 100 wt. %. Another marked disadvantage, mainly for trace elements analysis, is that the detection limits of Fe and Ni are significantly poorer than the detection limits usually attained during the analyses using 20 kV accelerating voltage. During our measurements, the average detection limits using 10 kV and 20 kV, respectively, were 3300 and 1950 ppm for Fe, 6800 and 1900 ppm for Ni, and 860 and 430 ppm for Cr. Although, in our analyses, Fe and Ni were present as major elements in terms of concentration, using low-U might not be suitable for trace elements analyses. The trend of higher detection limits with decreasing accelerating voltage is well-known (McSwiggen 2014). The analyst must be aware of the disadvantages and decide if the low-U method is suitable for planned measurements.

As stated above, the presence of the daubréelite lamellas may affect the analysis of troilite in various ways. Placing the point of analysis in a homogenous area might be difficult or even impossible in some cases. Some questions have arisen about the unequilibration in troilite composition (i.e., high compositional heterogeneity) compared to the equilibrated composition of silicates, especially in equilibrated enstatite chondrites (Fagan et al. 2022). Even though the possible heterogeneities in Cr concentration cannot be excluded, especially in the cases of unequilibrated chondrites like EH3 or EL3, the Cr contents might probably be affected by one of the phenomena causing the bias in Cr concentration in EPMA analyses. Moreover, it should be noted that though titanium represents the second most abundant trace element next to Cr, a similar trend was not seen in Ti concentrations in troilites of enstatite chondrites. However, the high variability in Ti concentration was documented in troilite analyses of aubrites. In the case of Ti enrichment of troilite in aubrites, tiny inclusions or lamellas were visible using FEG-SEM.

In general, it is challenging or nearly impossible to quantify the influence of the presence of tiny lamellas, sometimes combined with the boundary fluorescence on the EPMA analyses. However, the high variability in the data set and high extreme values might be promising markers of these phenomena. Unfortunately, the whole set of analyses and/or images documenting the places of analyses are usually not included in scientific papers, even within supplementary materials. Nevertheless, the high standard deviation of the data set, which is usually published, might be a good indicator that some of the results represent rather bulk analyses than compositions of a singular point.

5. Conclusions

Chromium and titanium enrichments in troilites of enstatite-rich meteorites are well-known. The presence of daubréelite lamellas in troilites of enstatite chondrites is also common knowledge in the meteorite research community. However, little attention was paid to the consequences of their presence on the measured chromium content of troilite. The current study showed that various mechanisms might occur and, alone or combined, influence the Cr concentration measured by EPMA in an unquantifiable amount.

The mechanisms for increasing Cr content include: a) The presence of the daubréelite lamellas (or inclusion) may have gone unnoticed due to its size or because it is located within the analytical volume beneath the surface of the sample. b) The boundary fluorescence from neighboring daubréelite can affect the measurements of the nearby troilite.

Enrichment in elements other than Cr, such as Mn or Mg, might be caused by tiny inclusions of (Mg,Fe,Mn) S-monosulfide; fortunately, the boundary fluorescence is not an issue in this case. Titanium concentration in troilite of aubrites was quite heterogeneous. Similarly to the troilites in the enstatite chondrites, Tiny Ti-rich inclusions were frequently found in such cases, mainly when using FEG-SEM for imaging. Moreover, other tiny inclusions or lamellas might influence other sulfides like (Mg,Fe,Mn)S-monosulfide as it sometimes contained small lamellas of the Fe-rich phase or troilite itself.

The influence of the inclusions or lamellas on the chemical composition of troilites cannot be quantified easily, so it is essential to know about their presence. Therefore, primary efforts put into the EPMA analyses of sulfides should be careful imaging, possibly with FEG-SEM if available, and avoiding unsuitable places for EPMA analysis. If applicable, we encourage using the low-U approach for iron (and possibly Ni), as described in the Methods section. This approach may help obtain a less affected dataset due to the smaller analytical volume

measured. However, using a low-U approach might not often be suitable. Given the complexity of the EPMA settings, we recommend specifying the measurement setup for a single type of sulfide or sulfides with similar chemical compositions. Regardless of whether the chemical composition is measured using a low-U approach or not, the most crucial aspect is to evaluate the dataset carefully and eliminate any biased data.

Acknowledgements. This research was supported by the Charles University Grant Agency project No. 1090119 (to NM) and the Institutional Research Plan No. RVO 67985831 of the Institute of Geology of the Czech Academy of Sciences, Prague. We would like to thank Akira Yamaguchi (NIPR) for the sample loan. Also, great gratitude goes to Petr Harcuba (MFF CU) for preparing TEM lamellas and conducting the SEM observation and to Jozef Veselý (MFF CU) for conducting the TEM study. We appreciate the thorough reviews by Makoto Kimura and the anonymous reviewer. Manuscript handling by Jiří Sejkora is highly acknowledged.

References

BAEDECKER PA, WASSON JT (1975) Elemental fractionations among enstatite chondrites. Geochim Cosmochim Acta 39: 735–765

BRETT R, KEIL K (1986) Enstatite chondrites and enstatite achondrites (aubrites) were not delivered from the same parent body. Earth Planet Sci Let 81: 1–6

Castaing R (1951) Application des sondes électronique à une méthode d'analyse ponctuelle chimique et cristallographique. PhD Thesis, University of Paris, 1952, Publication ONERA N. 55

DROUIN D, COUTURE AR, JOLY D, TASTET X, AIMEZ V, GAUVIN R (2007) CASINO V2.42 – A Fast and Easy-to-use Modeling Tool for Scanning Electron Microscopy and Microanalysis Users. Scanning 29: 92–101

Donovan J, Kremser D. Fournelle J, Goemann K (2012) Probe for EPMA: acquisition, automation and analysis. Probe Software, Inc., Eugene, Oregon

EL GORESY A, KULLERUD G (1969). Phase Relations in the System Cr–Fe–S. In: Millman PM (eds) Meteorite Research. Astrophysics and Space Science Library, vol 12. Springer, Dordrecht

EL GORESY A, YABUKI H, EHLERS K, WOOLUM D, AND PERNICKA E (1988) Qingzhen and Yamato-691: A tentative alphabet for the EH chondrites. Proc NIPR Symp Antarct Meteorites 1: 65–101

FAGAN TJ, KOMATSU M, NOGUCHI K, TOSHIMA S (2022) Equilibration in silicate (pyroxene) vs sulfide (troilite) during metamorphism of enstatite chondrites. Meteorit Planet Sci: 57: A129 (LPI Contributions No. 2695)

- HORSTMANN M, HUMAYUN M, BISCHOFF A (2014) Clues to the origin of metal in Almahata Sitta EL and EH chondrites and implications for primitive E chondrite thermal histories. Geochim Cosmochim Acta 140: 720–744
- IKEDA Y (1989) Petrochemical study of the Yamato-691 enstatite chondrite (E3) IV: Descriptions and mineral chemistry of opaque-mineral nodules. Proc NIPR Symp Antarct Meteorites 2: 109–146
- Kallemeyn GW, Wason JT (1986) Compositional of enstatite (EH3, EH4,5 and EL6) chondrites: Implications regarding their formation. Geochim Cosmochim Acta 50: 2153–2164
- Keil K (1969) Titanium distribution in enstatite chondrites and achondrites, and its bearing in their origin. Earth Planet Sci Let 7: 243–248
- Keil K (1986) Mineralogical and chemical relationships among enstatite chondrites. J Geophys Res 73 (22): 6945–6976
- Keil K (2007) Occurrence and origin of keilite, (Fe>0.5, Mg<0.5)S, in enstatite chondrite impact-melt rocks and impact-melt breccias. Chem Erde 67: 37–54
- Keil K (2010) Enstatite achondrite meteorites (aubrites) and the histories of their asteroidal parent bodies. Chem Erde: 295–317
- KEIL K, ANDERSEN CA (1965) Electron microprobe study of the Jajh deh Kot Lalu enstatite chondrite. Geochim Cosmochim Acta 29: 621–632
- Keil K, Fredriksson K (1963) Electron microprobe analysis of some rare minerals in the Norton County achondrite. Geochim Cosmochim Acta 27 (9): 939–947
- KEIL K, SNETSINGER KG (1967) Niningerite: A new Meteoritic sulfide. Science 155 (3761): 451–453 KIMURA M, LIN Y, IKEDA Y, EL GORESY A, YANAI K, KOJIMA H (1993) Mineralogy of antartic aubrites, Yamato-793592 and Allan Hills-781113: Comparison with non-antartic aubrites and E-chondrites. Proc NIPR Symp Antarct Meteorites 6: 186–203
- KIMURA M, YAMAGUCHI A, MIYAHARA M (2017) Shock-induced thermal history of an EH3 chondrite, Asuka 10164. Meteorit Planet Sci 52: 24–35
- KIMURA M, WEISBERG MK, TAKAKI A, IMAE N, YAMAGUCHI A (2021) An Almahata Sitta EL3 fragment: implications for the complex thermal history of enstatite chondrites. PEPS 8: 1–12
- LIN Y (2022) Enstatite chondrites: condensation and metamorphism under extremely reducing conditions and contributions to the Earth. PEPS 9: 28
- LIN Y, EL GORESY A (2002) A comparative study of opaque phases in Qingzhen (EH3) and MacAlpine Hills 88136 (EL3): Representatives of EH and EL parent bodies. Meteorit Planet Sci 37: 577–599
- LIN Y, KIMURA M (1998) Petrographic and mineralogical study of new EH melt rocks and a new enstatite chondrite grouplet. Meteorit Planet Sci 33: 501–511

- LLOVET X, SAVAT F (2017) PENEPMA: A Monte Carlo Program for the Simulation of X-Ray Emission in Electron Probe Microanalysis. Microsc Microanal 23(3): 634–646
- LLOVET X, PINARD PT, DONOVAN JJ, SALVAT F (2012) Secondary fluorescence in electron probe microanalysis of material couples. J Phys D Appl Phys 45: 225301
- MASON B (1966) The enstatite chondrites. Geochim Cosmochim Acta 30: 23–39
- McGee JJ, Keil K (2001) Application of electron probe Microanalysis to the study of geological and planetary materials. Microsc Microanal 7: 200–210
- McSwiggen P (2014) Characterization of sub-micrometer features with FE-EPMA. IOP Conf Ser Mater Sci Eng 55(1): 012009
- Meteoritical Bulletin Database; https://www.lpi.usra.edu/meteor/; editing status 2021-11-29; re3data.org Registry of Research Data Repositories DOI 10.17616/R3MM1Z last accessed from re3data.org: 2024-08-08
- Mészárosová N (2024) Chemical composition of sulfides from enstatite-rich meteorites. Mendeley Data V1 DOI 10.17632/29yn7d7bmj.1
- MÉSZÁROSOVÁ N, SKÁLA R (2022) Relationship of daubréelite with troilite: A study of troilites of enstatite chondrites at the nanoscale. Meteorit Planet Sci 57: S1 #6155
- MOY A, VON DER HANDT A, FOURNELLIE J (2022) Solving the iron quantification problem in low-kV EPMA: An essential step toward improved analytical spatial resolution in electron probe microanalysis Fe sulfides. Amer Miner 107: 1532–1544
- VAN NIEKERK D, KEIL K, HUMAYUN M (2014) Petrogenesis of anomalous Queen Alexandra Range enstatite meteorites and their relation to enstatite chondrites, primitive enstatite achondrites, and aubrites. Meteorit Planet Sci 49: 295–312
- PATZER A, SCHLÜTER J, SCHULTZ L, TARKIAN M, HILL DH, BOYNTON WV (2004) New findings for the equilibrated enstatite chondrite Grein 002. Meteorit Planet Sci 9: 1555–1575
- REED SJB (2005) Electron Microprobe Analysis and Scanning Electron Microscopy in Geology. 2nd ed. Cambridge: Cambridge University Press, pp 1–192
- RINALDI R, LLOVET X (2015) Electron probe microanalysis: A review of the past, present, and future. Microsc Microanal 21: 1053–1069
- SKINNER BJ, LUCE FD (1971) Solid solutions of the type (Ca,Mg,Mn,Fe)S and their use as geothermometers for the enstatite chondrites. Amer Miner 56: 1269–1296
- SWEATMAN TR, LONG JVP (1969) Standards and Correction Procedures in Electron-Probe Analysis of Rock-Forming Minerals. In: Möllenstedt G, Gaukler KH (eds) Vth International Congress on X-Ray Optics and Microanalysis / V. Internationaler Kongreß für Röntgenoptik und Mikroanalyse / Ve Congrès International sur l'Optique des Rayons X et la Microanalyse. Springer, Berlin, Heidelberg: 432–437

- UDRY A, WILBUR ZE, RAHIB RR, McCubbin FM, Vander Kadden KE, McCoy TJ, Ziegler K, Gross J, Defelice C, Combs L, Turrin BD (2019) Reclassification of four aubrites as enstatite chondrite impact melts: Potential geochemical analogs for Mercury. Meteorit Planet Sci 54: 785–810
- WATTERS TR, PRINZ M (1979) Aubrites: Their origin and relationship to enstatite chondrites. Proc Lunar Planet Sc Conf 10th: 1073–1093
- WEISBERG MK, KIMURA M (2012) The unequilibrated enstatite chondrites. Chem Erde 72: 101–115
- WEYRAUCH M, HORSTMANN M, BISCHOFF A (2018) Chemical variation of sulfides and metal in enstatite chondrites

 Introduction of a new classification scheme. Meteorit
 Planet Sci 53: 394–415
- WILBUR Z, UDRY A, MCCUBBIN FM, VANDER KAADEN KE, DEFELICE C, ZIEGLER K, ROSS DK, MCCOY TJ, GROSS J, BARNES JJ, DYGERT N, ZIEGLER RA, TURRIN BD, MCCOY C (2022) The effect of highly reduced magmatism revealed through aubrites. Meteorit Planet Sci 7: 1387–1420